Stability of Gravity Waves in the Presence of Surface Tension

Bernard Deconinck & Olga Trichtchenko
Department of Applied Mathematics
University of Washington
Seattle, WA 98195-3925

Abstract

The goal of this work is to investigate the effect of the inclusion of small surface tension on the instabilities of gravity water waves that are present even in shallow water [15]. Using the recent reformulation of Ablowitz, Fokas and Musslimani [1], we compute traveling water waves where the effects of both gravity and small surface tension are incorporated. The spectral stability of these solutions is examined using Hill's method [14]. It is found that the instabilities are not suppressed by the inclusion of surface tension. In fact, the growth rates associated with them increase as the surface tension grows. Generalizing the work of MacKay and Saffman [30], the persistence of these instabilities is confirmed analytically for waves of small amplitude.

1 Introduction

The classical water wave problem is the problem of determining the shape and dynamics of the free surface on a three-dimensional incompressible, inviscid fluid. If, in addition, the fluid is irrotational, a velocity potential may be introduced. Considering waves without variation in the second horizontal direction, the problem is described by the classical equations [38]

$$\begin{cases} \phi_{xx} + \phi_{zz} = 0, & (x,z) \in D, \\ \phi_z = 0, & z = -h,\ x \in (0,L), \\ \eta_t + \eta_x \phi_x = \phi_z, & z = \eta(x,t),\ x \in (0,L), \\ \phi_t + \dfrac{1}{2}\left(\phi_x^2 + \phi_y^2\right) + g\eta = \sigma \dfrac{\eta_{xx}}{\left(1+\eta_x^2\right)^{3/2}}, & z = \eta(x,t),\ x \in (0,L), \end{cases} \tag{1}$$

where h is the height of the fluid, g is the acceleration due to gravity and $\sigma > 0$ is the coefficient of surface tension[1]. Further, $\eta(x,t)$ is the elevation of the fluid surface, and $\phi(x,z,t)$ is its velocity potential. In this paper, we focus on solutions on a periodic domain $D = \{(x,z) \mid 0 \leq x < L, -h < z < \eta(x,t)\}$, see Fig. 1.

The work presented here follows that of Deconinck & Oliveras [15]. They presented a thorough numerical overview of the spectral instabilities of periodic traveling one-dimensional gravity (*i.e.*, $\sigma = 0$) water waves. An emphasis of that work is the presence of oscillatory instabilities even for waves in shallow water ($kh < 1.363$, see [5, 39], here $k = 2\pi/L$). Since the underlying waves are periodic, their stability analysis uses Hill's method, see [14], which incorporates the conclusions from Floquet's Theorem with Fourier analysis. This associates with each wave a range of Floquet exponents μ which may be taken as $(-\pi/L, \pi/L]$. The growth rates of the oscillatory instabilities is small, even for waves of moderate amplitude, and the range of Floquet exponents with which they are associated is narrow (on the order of 10^{-4} for $L = 2\pi$). A naive uniform distribution on $(-\pi/L, \pi/L]$ of Floquet exponents is bound to miss the presence of these instabilities, unless

[1] As noted in [4], $\sigma > 0$ for liquid-gas interfaces.

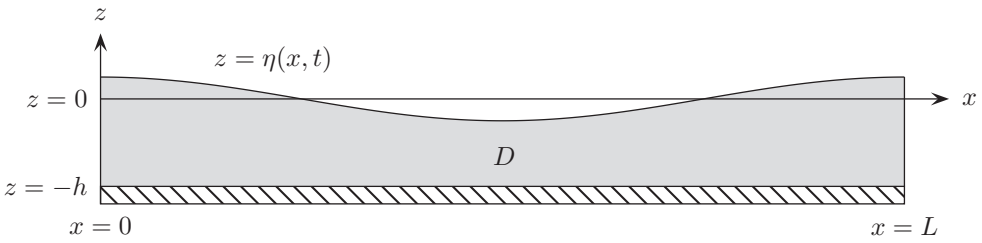

Figure 1: The domain on which we solve Euler's equations.

an exorbitantly large number of μ values are considered. Numerically, this is prohibitively expensive (often, no more than 100 μ-values are chosen), and an adaptive approach is used in [15], with more values of μ considered near those values of the Floquet exponents where instabilities may arise, as predicted by MacKay & Saffman [30].

Our goal is to investigate the effect of the inclusion of surface tension on the oscillatory instabilities. It is well known that the incorporation of capillary effects leads to the presence of resonances in the Fourier representation of the periodic traveling water waves. If the resonance condition is satisfied exactly, so-called Wilton ripples are found [38, 40]. Even when the condition is not met, its residual can be made arbitrarily small by the consideration of Fourier modes with sufficiently high wave number. This is especially problematic for waves of moderate or high amplitude, whose accurate Fourier representation requires more modes. This is discussed in more detail in Sections 4 and 5. Because of this, we limit our investigations to the instabilities of waves of small amplitude, so that (near-) resonance is avoided. Waves in both shallow and deep water are considered.

In the next section we provide an overview of the literature on this classical problem. Section 3 discusses the reformulation of the water wave problem we use, both for the computation of the traveling wave solutions, and for the analysis of their stability. After that, different sections are devoted to the computation of the solutions, and to the numerical investigation of their spectral stability. In addition, we revisit the work of MacKay & Saffman [30], which allows for an analytical prediction of which modes may lead to instabilities. We finish with conclusions.

2 Literature overview

The study of water waves goes back as far as Newton (1687), Euler (1761) and Bernouilli (1738) [11]. The study of water waves benefits from theoretical contributions in addition to experimental ones. This literature review attempts to cover the literature that is most relevant to the current work. It is by no means comprehensive. First, we discuss the history of the computation of traveling wave solutions to (1). Next, we review the literature on the investigation of their stability properties.

Stokes was the first to construct solutions to Euler's equations in 1847. He introduced a form for a graph of a traveling wave on a periodic domain [35]. This was done perturbatively by adding successive harmonics of a cosine profile. In 1880, he conjectured there is a gravity wave of maximum height that is achieved when the distance from crest to trough is 0.142 wavelengths [11]. The first papers to show that series expansion in powers of the wave amplitude (or Stokes expansions) converges were due to Nekrasov (1921) [33] and Levi-Civita (1925) [24]. They showed that the Stokes series converges when the ratio of amplitude to wavelength is sufficiently small and the waves are in infinitely deep water. Struik (1926) [36] extended this analysis for water of finite depth.

Examining periodic surface gravity-capillary waves using an expansion like the one used by Stokes, Wilton (1915) [40] computed successive coefficients, while including the effects of surface tension. He showed that if the coefficient of surface tension in deep water is proportional to the inverse of an integer, the denominator of the expansion coefficients becomes zero. Since the terms of the series are computed only up to a scaling,

he postulated that by choosing this scaling constant proportional to the vanishing denominator, convergence of the series may once again be achieved.

Following Stokes's conjecture of a wave of greatest height for gravity waves [35], Crapper [12] investigated the possibility of a wave of maximum height for purely capillary waves. Using a series expansion similar to Stokes (1957), he wrote down an exact solution for capillary waves of arbitrary amplitude on an infinitely deep fluid, and concluded a similar result was possible for finite depth. He found that for infinite depth, the wave of greatest height occurs when the distance from crest to trough is 0.73 wavelengths. A good overview of results on the computation of traveling wave solutions, including many results not discussed here, is found in the recent monograph by Vanden-Broeck [38]. Many of the results detailed there show the intricacies that follow from the inclusion of surface tension.

With solutions to Euler's equations on the periodic domain in hand, it is important to address their stability. Phillips (1960) [19] examined the dynamics of gravity waves on the surface of deep water and realized that when certain conditions are met, the waves behave as forced, resonant oscillators which cause energy transfer between the constituting wave trains. This work was supported by many experimental and numerical results such as the ones by Longuet-Higgins [28] and others. Phillips focussed on a perturbation series expansion and the conditions necessary for the higher-order terms to satisfy the linear dispersion relation. He predicted that resonant triads are not possible for gravity waves in deep water. McGodrick showed such triads are possible when surface tension is incorporated [19]. This was followed in 1967 by the works of Benjamin [5] and Whitham [39], who derived the criterion that Stokes waves on sufficiently deep water, *i.e.*, $kh > 1.363$ with $k = 2\pi/L$, are modulationally unstable. For $kh < 1.363$, this instability is not present.

In 1968, these efforts were followed by the seminal work of Zakharov [41]. Starting from Euler's equations, he showed that the water wave problem is Hamiltonian. He wrote the energy in terms of the canonical variables $\eta(x,t)$ and $q(x,t) = \phi(x,\eta(x,t),t)$. Truncating in powers of the wave amplitude, he derived what is now called the Zakharov equation, from which the Nonlinear Schrödinger equation easily follows. This equation describes the dynamics of a modulationally unstable wave train, and in this sense predicts what happens after the onset of the Benjamin-Feir instability.

By linearizing around a steady state solution, a stability eigenvalue problem is obtained whose spectrum determines the spectral stability of that solution. By examining the collision of eigenvalues in this spectrum, McLean (1982) [31] separated the instabilities in two classes. Building on numerical work of Longuet-Higgins [25, 26] and others, he obtained the maximal growth rates for different instabilities as a function of wave steepness. Exploiting the Hamiltonian nature of the problem [41], MacKay and Saffman (1986) [30] established necessary criteria for the onset of different instabilities as the amplitude of the solution is increased, within the framework of the general theory of Krein signatures [29]. These results are used below.

Many different ways of reformulating Euler's equations exist, mainly aimed at avoiding having to solve Laplace's equation in an unknown domain. The conformal mapping method is used to solve the one-dimensional water wave problem and leads to equations such as the ones used by Longuet-Higgins and Cokelet (1976) [28]. Another approach uses the canonical coordinates introduced by Zakharov [41], and defines a Dirichlet-to-Neumann operator, see Craig and Sulem (1993) [10]. Akers and Nicholls (2010) use the "Transformed Field Expansion" method, and they include the effects of surface tension [2]. Since we build on the work of Deconinck and Oliveras (2011) [15], the method most relevant to us is the reformulation due to Ablowitz, Fokas and Musslimani (2006) [1]. In this paper, the water wave problem is rewritten as two coupled equations, one local and one nonlocal. Since this is the basis for our work, this method is discussed below in some detail. The solutions of Deconinck and Oliveras [15] are in the form of a cosine series whose coefficients vary as the amplitude of the solution is increased. In [15], the effects of surface tension are not included. The stability of the solutions is analyzed using the Fourier-Floquet-Hill method [13, 14]. Deconinck and Oliveras show that, in addition to the Benjamin-Feir instability, there are bubbles of instability which show up more prominently as the amplitude of the solution is increased. These bubbles are shown to exist where the condition for the onset of instabilities due to MacKay and Saffman [30] is met. In shallow water (for $kh < 1.363$), they are found to be the only instabilities.

With the inclusion of surface tension, the majority of the results on stability for solutions of the water wave

problem focus on solutions defined on the whole line. Longuet-Higgins (1988) demonstrated numerically that the limiting capillary-gravity waves exist in deep water [27]. It was found that solitary waves of depression are stable and solitary waves of elevation are unstable for small steepness. The solutions become stable at finite steepness, see Calvo and Akylas (2001) [8]. The computation of solutions for gravity-capillary solitary waves was extended to two (surface) dimensions by Parau *et al.* (2004) [34] in infinite depth. It was found that these waves are unstable to perturbations transverse to the direction of propagation, but are stable to perturbations along the direction of propagation by Kim and Akylas (2007) [23]. Milewski *et al.* (2010) [32] analyzed the dynamics of interacting solitary waves.

Some results on the stability of periodic waves with surface tension can be found. Both Zhang and Melville [42] and Choi and Tiron [37] consider high surface tension, relative to the effect of gravity. In fact, for [37], $g = 0$, as they investigate the stability of Crapper's solutions [12]. More recently, and most relevant to the present work, Akers and Nicholls [2, 3] examine the spectral stability of traveling gravity-capillary waves, using the method of transformed field expansions. In [2], eigenvalues are not allowed to collide. As a consequence, the onset of instability can be predicted (when eigenvalues collide), but such instabilities cannot be tracked through the collision. This restriction is lifted in [3]. In both papers, the authors focus on perturbations of a prescribed (quasi-) period (not necessarily equal to the period of the underlying traveling wave), as the amplitude of the solution is increased. In our work, no perturbation period is prescribed, leading to a more comprehensive view of the spectral instabilities.

3 Reformulation

The reformulation of (1) of Ablowitz, Fokas and Musslimani [1] follows the work of Zakharov [41] by writing the water wave problem in terms of just the surface variables $\eta(x,t)$ and $q(x,t) = \phi(x,\eta(x,t),t)$, the velocity potential evaluated at the surface. Ablowitz, Fokas and Musslimani [1] show that the two functions $\eta(x,t)$ and $q(x,t)$ satisfy the system

$$q_t + \frac{1}{2}q_x^2 + g\eta - \frac{1}{2}\frac{(\eta_t + \eta_x q_x)^2}{1+\eta_x^2} = \sigma\frac{\eta_{xx}}{(1+\eta_x^2)^{3/2}}, \tag{2}$$

$$\int_0^L e^{ikx}\left[i\eta_t \cosh(k(\eta+h)) + q_x \sinh(k(\eta+h))\right]dx = 0, \quad \forall k \in \Lambda, \tag{3}$$

where $\Lambda = \{2\pi n/L \mid n \in \mathbb{Z},\ n \neq 0,\}$. In [1], only the whole line case is treated. The extension to the periodic case is straightforward [15].

Following the derivation of Deconinck and Oliveras [15], we transform to a traveling frame of reference, moving with speed c. Thus implies the substitution $x \to x - ct$, $\eta_t \to \eta_t - c\eta_x$ and $q_t \to q_t - cq_x$. The local and nonlocal equations (2) and (3) become

$$q_t - cq_x + \frac{1}{2}q_x^2 + g\eta - \frac{1}{2}\frac{(\eta_t - c\eta_x + \eta_x q_x)^2}{1+\eta_x^2} = \sigma\frac{\eta_{xx}}{(1+\eta_x^2)^{3/2}}, \tag{4}$$

$$\int_0^L e^{ikx}\left(i(\eta_t - c\eta_x)\cosh(k(\eta+h)) + q_x \sinh(k(\eta+h))\right)dx = 0, \quad k \in \Lambda. \tag{5}$$

Traveling wave solutions are stationary in this frame of reference, thus $q_t = 0 = \eta_t$. We solve for q_x using the local equation:

$$q_x = c - \sqrt{(1+\eta_x^2)\left(c^2 - 2g\eta + 2\sigma\frac{\eta_{xx}}{(1+\eta_x^2)^{3/2}}\right)}, \tag{6}$$

where we have chosen the negative sign in front of the square root [9]. Substituting in the nonlocal equation (5), integrating by parts and simplifying, we are left with

$$\int_0^L e^{ikx}\sqrt{(1+\eta_x^2)\left(c^2-2g\eta+2\sigma\frac{\eta_{xx}}{(1+\eta_x^2)^{3/2}}\right)}\sinh(k(\eta+h))dx=0,\quad k\in\Lambda. \tag{7}$$

Alternatively,

$$\int_0^L e^{ikx}\sqrt{(1+\eta_x^2)\left(c^2-2g\eta+2\sigma\frac{\eta_{xx}}{(1+\eta_x^2)^{3/2}}\right)}\left(\sinh(k\eta)+\cosh(k\eta)\tanh(kh)\right)dx=0,\quad k\in\Lambda, \tag{8}$$

where we have separated the explicit dependence on the depth h. This is useful for numerical purposes, and it allows for an easy limit when considering the case of water of infinite depth. Indeed, in the limit $h\to\infty$, (8) gives

$$\int_0^L e^{ikx}\sqrt{(1+\eta_x^2)\left(c^2-2g\eta+2\sigma\frac{\eta_{xx}}{(1+\eta_x^2)^{3/2}}\right)}e^{|k|\eta}dx=0,\quad k\in\Lambda. \tag{9}$$

In what follows, we equate the solution period L to 2π. Thus $\Lambda=\{n\mid n\in\mathbb{Z},\ n\neq 0,\}$.

4 Constructing traveling-wave solutions

We construct solutions to (8) (or (9)) using numerical continuation. AUTO [16] and MatCont [18] are often used for this purpose. For our equations these software packages are difficult to use because of the nonlocality present. Instead, we wrote our own continuation program. The trivial solution $\eta=0$ satisfies (8) for all values of c. At particular values of the wave speed c the equation admits nontrivial solutions as well, and bifurcation branches emanate. To determine these values of c, we linearize (8):

$$\int_0^{2\pi} e^{ikx}\left[c^2\eta+\left(-g\eta+\sigma\eta_{xx}\right)\frac{\tanh(kh)}{k}\right]dx=0,\quad k\in\Lambda. \tag{10}$$

With[2]

$$\eta=\sum_{n=1}^{\infty}a_n\cos(nx),$$

the linearized equation becomes

$$\left[c^2-\left(g+k^2\sigma\right)\frac{\tanh(kh)}{k}\right]a_k=0,\quad k\in\Lambda. \tag{11}$$

We impose that for $k=1$, the factor in brackets is zero, so that

$$c=\sqrt{(g+\sigma)\tanh(h)}, \tag{12}$$

and a_1 is not forced to be zero. Then, for almost all values of σ,

$$\eta=a_1\cos(x), \tag{13}$$

[2]This form of η equates the average of the free surface to zero, without loss of generality.

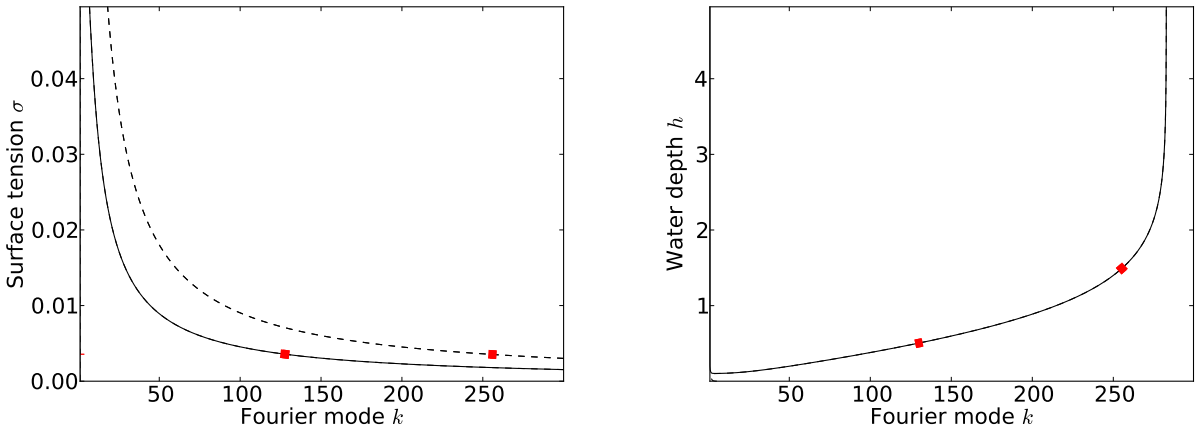

(a) (b)

Figure 2: Figure 2a displays the solution set of the resonance condition for different Fourier modes k and different values of the coefficient of surface tension, for both deep (solid curve) and shallow water (dashed curve). The red dots indicate the resonant k values for $\sigma = 1/(90\pi)$. Figure 2a displays the solution set as a function of depth h and wave number k, for $\sigma = /(90\pi)$ and the red dots correspond to the values of the depth we use, $h = 0.5$ (shallow water) and $h = 1.5$ (deep water).

where a_1 is an arbitrary constant. Near $c = \sqrt{(g+\sigma)\tanh(h)}$, (8) with a_1 sufficiently small, is an accurate representation of the solution. To compute $\eta(x)$ as we continue up the branch, we use Newton's method in Fourier space as described below. This results in a finite-term Fourier representation of the solution, which is truncated at whatever order guarantees the numerical accuracy desired.

There are particular values of σ for which the factor in parentheses of (11) is zero for a second value of $k \neq 1$, once c has been chosen as in (12). In this case, the linear solution consists of two terms, leading to resonant solutions or Wilton ripples [38]. Since the goal of our work is to examine the effect of small surface tension on gravity waves, we wish to stay away from the resonance phenomenon. The factor seen in (11) appears at all orders. More explicitly, the resonance condition is given by

$$(g+\sigma)\tanh(h) - \left(g + k^2\sigma\right)\frac{\tanh(kh)}{k} = 0. \tag{14}$$

This equation can be solved (numerically) for k, as a function of g, h, and σ. For most parameter values, the solution k is not an integer, implying that resonance does not occur. However, for computational purposes we need to avoid near resonances as well. Near resonances occur for integer values of k near the solution of (14). This leads to small denominators in terms with these wave numbers in the Fourier series of the solution, which presents numerical difficulties, unless their numerators are even smaller[3]. Thus, in order to have a well-resolved solution, we need to stay away from Fourier modes that satisfy (14) or for which the residual of this equation is small.

For fixed g and two different values of h ($h = 0.5$, shallow water, dashed line, and $h = 1.5$, deep water, solid line), Figure 2a displays the solution of (14) in the (k, σ) plane. For instance, the figure shows that for $\sigma = 1/(90\pi)$, near resonance and the small-denominator problem in the Fourier series occur near the 125th and the 260th mode for deep and shallow water respectively. Provided that the desired accuracy of the solution under consideration is achieved with far fewer terms, near resonance is not a problem. For our purposes, we let $\sigma = 1/(90\pi)$, and we consider solutions that require never more than 100 terms in their

[3]This happens if the near-resonance occur for sufficiently high wave number terms, which are not necessary for the accurate numerical evaluation of the series

Fourier expansion to achieve the numerical accuracy desired. This imposes a *de facto* restriction on the amplitude of the solution we consider, while allowing for solutions that, although not of maximal amplitude, are decidedly in the nonlinear regime. It should be noted that for $\sigma = 0$, resonance is not possible. Also, in the limit of water of infinite depth, resonance occurs for $k = g/\sigma$.

4.1 Numerical Implementation

In order to construct the solutions numerically, using a continuation method, we truncate the number of Fourier modes of the solution to a finite integer N. Let

$$\eta_N(x) = \sum_{j=1}^{N} a_j \cos(jx). \tag{15}$$

Recall that the nonlocal equation (8) is valid for every integer $k \neq 0$. We truncate the number of equations to N so that $k = 1, \ldots, N$. However the speed c at which the wave moves is an additional unknown. Thus an extra equation is required. Different options are possible and their convenience is dictated by how we parameterize the solution bifurcation branch. If we parametrize using a_1, then we can either prescribe a_1 as a variable or we can add the equation

$$a_1 - \tilde{a}_1 = 0,$$

where $\tilde{a}_1$ is a prescribed value, determining the next solution on the bifurcation branch. Parameterizing using a_1 is a convenient and justifiable choice for solutions of small amplitude. As the amplitude is increased, this may cease to be the case, but since we are limiting ourselves to solutions of small and moderate amplitude, this is not an issue for us. Alternatively, one could prescribe the L^2 or L^∞ norm of the solution, as was done in [15]. In any case, we end with $N + 1$ equations determining $N + 1$ unknowns.

Remark. We may overdetermine the number of equations so as to solve a least-squares problem. However, this requires the use of additional values of $k > N$. Since for large values of k, the cosh and sinh contributions in the nonlocal equation become large exponentially fast this must be done with care to control numerical error.

Denote the vector of unknowns as

$$z = [c, a_1, a_2, a_3, \ldots, a_N]^T.$$

Equating

$$F^{(N)}(z) = [a_1 - \tilde{a}_1, F_1(z), F_2(z), \ldots, F_N(z)]^T,$$

where $\tilde{a}_1$ is given as a small increment of the value at the previous solution, and

$$\begin{aligned} F_j^{(N)}(z) &= \int_0^{2\pi} e^{ijx} \sqrt{\left(1 + \eta_{N,x}^2\right)\left(c^2 - 2g\eta_N + 2\sigma \frac{\eta_{N,xx}}{(1+\eta_{N,x}^2)^{3/2}}\right)} (\sinh(k\eta_N) + \cosh(k\eta_N)\tanh(kh))dx \\ &= \int_0^{2\pi} f_j(k, c, \eta_N, \eta_{N,x}, \eta_{N,xx})dx, \end{aligned}$$

which defines $f_j(k, c, \eta_n, \eta_{N,x}, \eta_{N,xx})$. We wish to solve $F^{(N)}(z) = 0$ for the unknown vector z. Using Newton's Method, the n-th iteration is given by

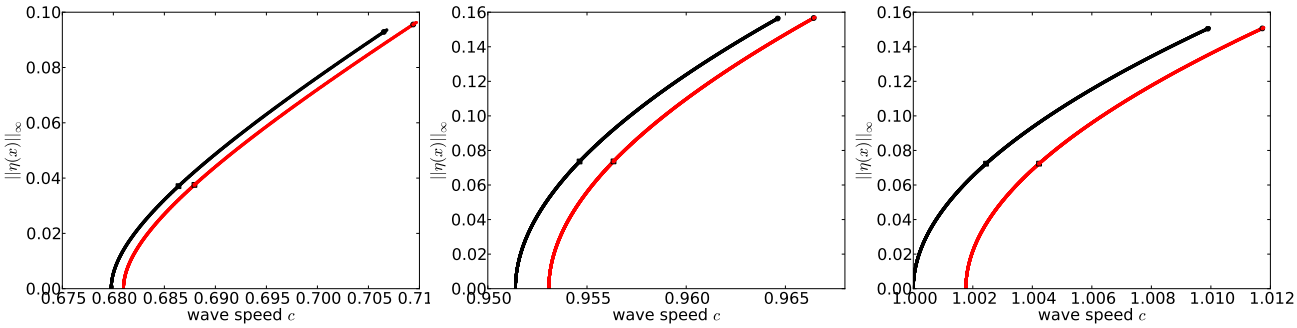

(a) (b) (c)

Figure 3: The solution bifurcation branches for pure gravity waves ($\sigma = 0$, black) and gravity-capillary waves ($\sigma = 1/(90\pi)$, red) for (a) shallow water, $h = 0.5$, (b) deep water, and (c) water of infinite depth.

$$z^{n+1} = z^n - J^{-1}(z^n)F(z^n),$$

where J is the Jacobian with entries

$$(J)_{jl} = \frac{\delta F_j}{\delta z_l} = \int_0^{2\pi} \left(\frac{\partial f_j}{\partial z_l} + \frac{\partial f_j}{\partial \eta_N}\frac{\partial \eta_N}{\partial z_l} + \frac{\partial f_j}{\partial \eta_{N,x}}\frac{\partial \eta_{N,x}}{\partial z_l} + \frac{\partial f_j}{\partial \eta_{N,xx}}\frac{\partial \eta_{N,xx}}{\partial z_l} \right) dx,$$

which is readily computable. Our continuation method starts from flat water, after which we proceed to follow the bifurcation branch with initial guess

$$[\sqrt{(g+\sigma)\tanh(h)}, \tilde{a}_1, 0, 0, 0, \ldots, 0]^T.$$

This initial guess is modified as we proceed up the branch. Python and Matlab both are used to implement the numerical scheme. To check the convergence of the algorithm, we check the residual error as well as the decay in the Fourier modes of the solution. Results are given below. The continuation is started using N=20 Fourier modes only, due to the small amplitude of the solution. Only a few of the 20 modes are distinguishable from 0 initially. As the bifurcation parameter is increased, more than 20 modes are needed to accurately represent the solution. The value of N is increased acoordingly, *i.e.*, more equations are used, depending on more unknowns. This is limited by the presence of the exponentially growing functions, which is why we work with solutions that are accurately represented using no more than 100 Fourier modes. Throughout the exponential decay of the Fourier amplitudes that is expected of an analytic solution profile is checked, ensuring that the computed modes with highest wave number have neglible (less than 10^{-14}) Fourier amplitude.

4.2 Numerical Results

We compare the computed traveling wave profiles for particular values of the depth h, with and without surface tension. The value $\sigma = 1/(90\pi)$ is used throughout. The solution bifurcation branches are shown in Figure 3. The case of no surface tension is shown in black, while $\sigma = 1/(90\pi)$ is red. This convention is used throughout the paper. The top row of Figure 4 displays the actual solution profile, divided by $\eta(0)$, to allow for the comparison of profiles of different amplitudes. Different columns show the results for different depth h, with $h = 0.5$, $h = 1.5$, and $h = \infty$ in order. The bottom row of Figure 4 shows the exponential decay of the Fourier coefficients of the computed solutions. It is clear that the effect of small surface tension

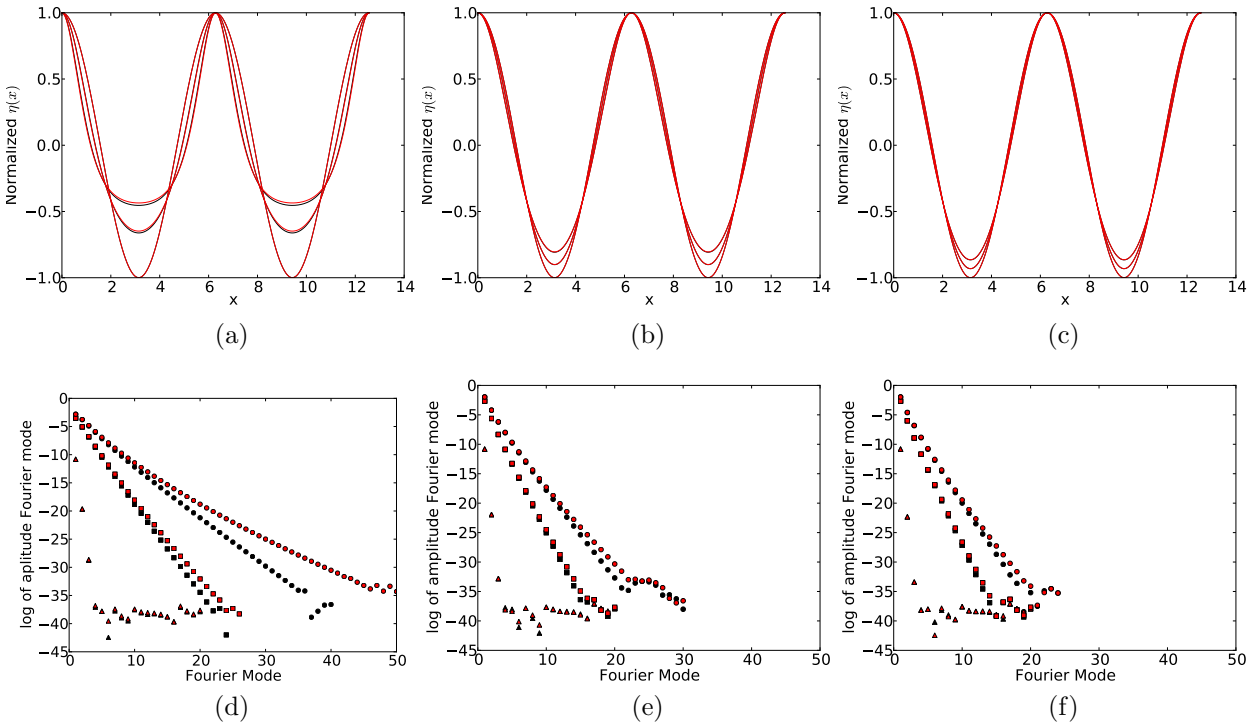

Figure 4: Solution profiles $\eta(x)/\eta(0)$ for (a) shallow water, $h = 0.5$, (b) for deep water, $h = 1.5$, and (c) for water of infinite depth, $h = \infty$. Note that in deep water, the profiles of pure gravity waves (black) and gravity-capillary waves (red) with $\sigma = 1/(90\pi)$ are almost indistinguishable. The exponential decay of the Fourier modes for the corresponding solutions is shown in the bottom row.

on the solution profile is perturbative only: no qualitative changes are discernible and quantitative changes are small.

In the top row of Figure 4, normalized wave profiles with higher troughs correspond to solutions higher on the bifurcation branches of Figure 4. Those solutions are also the profiles for which the decay of the Fourier amplitudes is the slowest. Accordingly, the Fourier representation of the profile requires more terms for comparable numerical accuracy. It appears that the inclusion of surface tension requires more Fourier modes for the accurate representation of the solution.

5 Stability

Next, we consider the spectral stability of these solutions. Our main interest is in comparing these results with those of Deconinck and Oliveras [15], where $\sigma = 0$. Since our traveling wave solutions are periodic, we use the Fourier-Floquet-Hill method [14] and follow the setup of [15]. Spectral stability of a solution is defined as

Definition 1. *(**Spectral Stability**). The equilibrium solution $u_0(x)$ of a dynamical system $u_t = \mathcal{N}(x, u, u_x, \ldots)$ is spectrally stable if the spectrum of the linear operator obtained by linearizing $\mathcal{N}$ around $u_0(x)$ has no strictly positive real part.*

This implies that perturbations of this solution do not exhibit exponential growth. Assume we have a linear operator $\mathcal{L}$ with elements λ of its spectrum such that

$$\mathcal{L}v = \lambda v.$$

The spectrum of a linear operator is defined in the standard way [20]:

Definition 2. ***(Spectrum of a Linear Operator)****. The spectrum of the linearized operator $\mathcal{L}$ is given by*

$$\sigma(\mathcal{L}) = \{\lambda \in \mathbb{C} : ||v(x)||_\infty < \infty\}. \tag{16}$$

For our purposes, the norm $||\cdot||_\infty$ denotes the infinity norm. Let the form of the solution to the equations (4) and (5) in the traveling frame of reference be

$$q(x,t) = q_0(x) + \epsilon q_1(x)e^{\lambda t} + O(\epsilon^2), \tag{17}$$
$$\eta(x,t) = \eta_0(x) + \epsilon \eta_1(x)e^{\lambda t} + O(\epsilon^2), \tag{18}$$

where η_0 is obtained from the numerical scheme described in the previous section and q_0 follows from (6). Since the water wave problem is Hamiltonian [41] the spectrum (16) of any traveling wave solution is symmetric with respect to both the real and imaginary axes. Thus, in order for the solution to be spectrally stable, it is necessary for the spectrum to be on the imaginary axis, *i.e.*, $Re\{\lambda\} = 0$, for all λ in $\sigma(\mathcal{L})$.

We do not restrict the period of the perturbations q_1 and η_1, which is possible by using Floquet's Theorem [21, 14]. For our problem, this implies that perturbations may be decomposed as

$$q_1(x) = e^{i\mu x}\tilde{q}_1, \quad \eta_1(x) = e^{i\mu x}\tilde{\eta}_1, \tag{19}$$

where $\mu \in [-1/2, 1/2)$ is the Floquet exponent and $\tilde{q}_1$, $\tilde{\eta}_1$ are periodic with period 2π. It is straightforward to apply the Floquet Theorem to the local equation, but the nonlocal case requires modification: before perturbing (5) using perturbations of the form (19) with arbitrary period, we replace the integral over one period by the average over the whole line [15]:

$$\langle f(x)\rangle = \lim_{M\to\infty} \frac{1}{M}\int_{-M/2}^{M/2} f(x)dx, \tag{20}$$

which is defined for almost periodic $f(x)$, which includes (quasi-) periodic $f(x)$ as in (19) [7]. The generalized local equation is identical to the previous one if the integrand is periodic.

5.1 The Generalized Eigenvalue Problem

We linearize the following system of equations about a traveling wave solution:

$$q_t - cq_x + \frac{1}{2}q_x^2 + g\eta - \frac{1}{2}\frac{(\eta_t - c\eta_x + q_x\eta_x)^2}{1+\eta_x^2} = \sigma\frac{\eta_{xx}}{(1+\eta_x^2)^{3/2}}, \tag{21}$$
$$\lim_{M\to\infty}\frac{1}{M}\int_{-M/2}^{M/2} e^{ikx}\left[i(\eta_t - c\eta_x)\cosh(k(\eta+h)) + q_x\sinh(k(\eta+h))\right]dx = 0, \quad k\in\Lambda. \tag{22}$$

Using (17-18), ignoring terms of $O(\epsilon^2)$ and higher, and dropping the tildes, we obtain

$$\begin{aligned}\lambda\left(f\eta_1 - q_1\right) = {} & (q_{0,x}-c)\mathcal{D}_x q_1 + g\eta_1 - f\left[(q_{0,x}-c)\mathcal{D}_x\eta_1 + \eta_{0,x}\mathcal{D}_x q_1\right] + f^2\eta_{0,x}\mathcal{D}_x\eta_1 \\ & - \sigma\frac{\mathcal{D}_x^2\eta_1}{1+\eta_{0,x}^{3/2}} + \sigma\frac{3\eta_{0,xx}\eta_{0,x}\mathcal{D}_x\eta_1}{(1+\eta_{0,x}^2)^{5/2}},\end{aligned} \tag{23}$$
$$\lambda\left\langle e^{ikx}\left[-i\mathcal{C}_k\eta_1\right]\right\rangle = \left\langle e^{ikx}\left[-i\mathcal{C}_k c\mathcal{D}_x\eta_1 + \mathcal{S}_k\mathcal{D}_x q_1 + \left(-i\eta_{0,x}c\mathcal{S}_k + q_{0,x}\mathcal{C}_k\right)k\eta_1\right]\right\rangle, \tag{24}$$

where

$$f(\eta_0, q_0) = \frac{\eta_{0,x}(q_{0,x} - c)}{1 + \eta_{0,x}^2}, \qquad \mathcal{D}_x = i\mu + \partial_x,$$
$$\mathcal{S}_k = \sinh(k(\eta_0 + h)), \qquad \mathcal{C}_k = \cosh(k(\eta_0 + h)), \qquad \mathcal{T}_k = \tanh(k(\eta_0 + h)).$$

Since q_1 and η_1 are periodic with period 2π,

$$q_1 = \sum_{m=-\infty}^{\infty} Q_m e^{imx}, \quad \eta_1 = \sum_{m=-\infty}^{\infty} N_m e^{imx}, \tag{25}$$

with

$$Q_n = \frac{1}{2\pi}\int_0^{2\pi} e^{-inx} q_1(x)dx, \qquad N_n = \frac{1}{2\pi}\int_0^{2\pi} e^{-inx}\eta_1(x)dx. \tag{26}$$

Truncating to the $2N+1$ Fourier modes from $-N$ to N, we define

$$U(x) = \left[N_{-N}(x), \ldots, N_0(x), \ldots, N_N(x), Q_{-N}(x), \ldots Q_0(x), \ldots, Q_N(x)\right]^T. \tag{27}$$

This leads to the finite-dimensional generalized eigenvalue problem

$$\lambda \mathcal{L}_1 U(x) = \mathcal{L}_2 U(x). \tag{28}$$

where

$$\mathcal{L}_1 = \begin{bmatrix} A & -I \\ C & 0 \end{bmatrix}, \quad \mathcal{L}_2 = \begin{bmatrix} S & T \\ U & V \end{bmatrix} \tag{29}$$

with I and 0 the $(2N+1)\times(2N+1)$ identity and zero matrix, respectively. The blocks A, S and T originate from the local equation, while C, U and V come from the nonlocal equation. Their matrix entries are

$$A_{m,n} = \frac{1}{2\pi}\int e^{i(m-n)x} f dx, \quad C_{m,n} = -i\frac{1}{2\pi}\int e^{i(m-n)x}\mathcal{C}_{\mu+m}dx,$$
$$S_{m,n} = -\frac{1}{2\pi}\int e^{i(m-n)x}\left[-g + f(q_{0x} - c)i(\mu + (m-N)) - f^2\eta_{0x}i(\mu + (m-N))\right.$$
$$\left. + \sigma\frac{-(\mu + (m-N))^2}{1+\eta_{0x}^2} - \sigma\frac{2\eta_{0xx}\eta_{0x}i(\mu + (m-N))}{(1+\eta_{0x}^2)^2}\right]dx,$$
$$T_{m,n} = \frac{1}{2\pi}\int e^{i(m-n)x}\left[(q_{0x} - c)i(\mu + (m-N)) - f\eta_{0x}i(\mu + (m-N))\right]dx,$$
$$U_{m,n} = \frac{1}{2\pi}\int e^{i(m-n)x}\left[S_{\mu+m}i(\mu + (m-N))\right]dx,$$
$$V_{m,n} = \frac{1}{2\pi}\int e^{i(m-n)x}\left[-ic(\mu + (m-N))\mathcal{C}_k + k(-i\eta_{0x}c\mathcal{S}_{\mu+m}) + q_{0x}\mathcal{C}_{\mu+m}\right]dx.$$

Lastly,

$$\mathcal{C}_{\mu+m} = \cosh((\mu+m)\eta_0) + \mathcal{T}_{\mu+m}\sinh((\mu+m)\eta_0), \quad \mathcal{S}_{\mu+m} = \sinh((\mu+m)\eta_0) + \mathcal{T}_{\mu+m}\cosh((\mu+m)\eta_0),$$

with $\mathcal{T}_{\mu+m} = \tanh((\mu+m)h)$. All block matrices in (29) are of size $(2N+1)\times(2N+1)$ with N the number of modes we retain. The convergence properties of the Floquet-Fourier-Hill method as $N \to \infty$ are discussed in [13, 22].

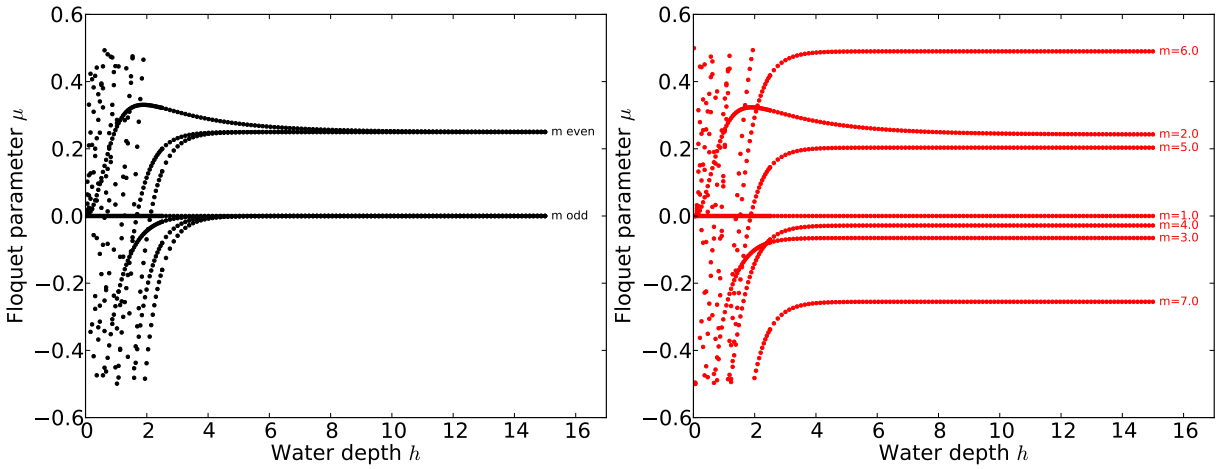

(a) (b)

Figure 5: Values of the Floquet exponent μ for which the collision condition is met, as a function of depth h. As before, black curves correspond to $\sigma = 0$, while curves in red are for $\sigma = 1/90\pi$. Different curves are obtained for different values of m, as indicated. As h is increased, only two different values of μ for which small amplitude instabilities may exist are approached asymptotically when $\sigma = 0$: $\mu = 0$ and $\mu = 1/4$. With $\sigma = 1/(90\pi)$ this is not the case and small amplitude solutions are potentially unstable with respect to perturbations of many different periods.

5.2 A Necessary Condition for Instabilities

Since the traveling wave solutions of Section 4 are constructed through numerical continuation from the trivial flat water state, it is natural to begin by considering the spectral stability of the flat water state. This is conveniently done using the Hamiltonian form of the problem, following Mackay and Saffman [30] and using notions from resonant interaction theory, as in [31]. These concepts are particularly easy to use in the flat water case, since the spectral problem (23-24) is one with constant coefficients. It is well known that spectral elements corresponding to different Floquet exponents do not interact, thus we may restrict our attention to a fixed μ value. It may be convenient to not restrict μ to the unit interval around the origin, keeping in mind that values of μ that have the same non-integer part are equivalent.

For flat water, $\eta_0 \equiv 0$, $q_0 \equiv 0$, and the spectral problem (23-24) becomes

$$\begin{aligned} \lambda\left(-q_1\right) &= (-c)\mathcal{D}_x q_1 + g\eta_1 - \sigma\mathcal{D}_x^2\eta_1, \\ \lambda\left(-i\mathcal{C}_{\mu+m}\eta_1\right) &= -i\mathcal{C}_{\mu+m}c\mathcal{D}_x\eta_1 + \mathcal{S}_{\mu+m}\mathcal{D}_x q_1. \end{aligned}$$

This system is easily solved, and the eigenvalues are explicitly given by

$$\lambda^s_{\mu+m} = ic(\mu+m) + is\sqrt{\left[g(\mu+m) + \sigma(\mu+m)^3\right]\mathcal{T}_{\mu+m}}, \tag{30}$$

with $s = \pm 1$. At this point the assumption $\sigma > 0$ mentioned in the footnote on page 1 is shown to be vital: if $\sigma < 0$ it is clear that the flat water state is not spectrally stable, and we end up with a variety of nonphysical and unobserved instabilities for surface water waves. With this assumption, all eigenvalues are on the imaginary axis and the flat water state is spectrally stable. The spectrum of (23-24) is a continuous function of the parameters appearing in $\mathcal{L}_1$ and $\mathcal{L}_2$ [20], including the traveling wave amplitude. In order for eigenvalues to leave the imaginary axis, they have to do so in pairs, symmetric with respect to both the real

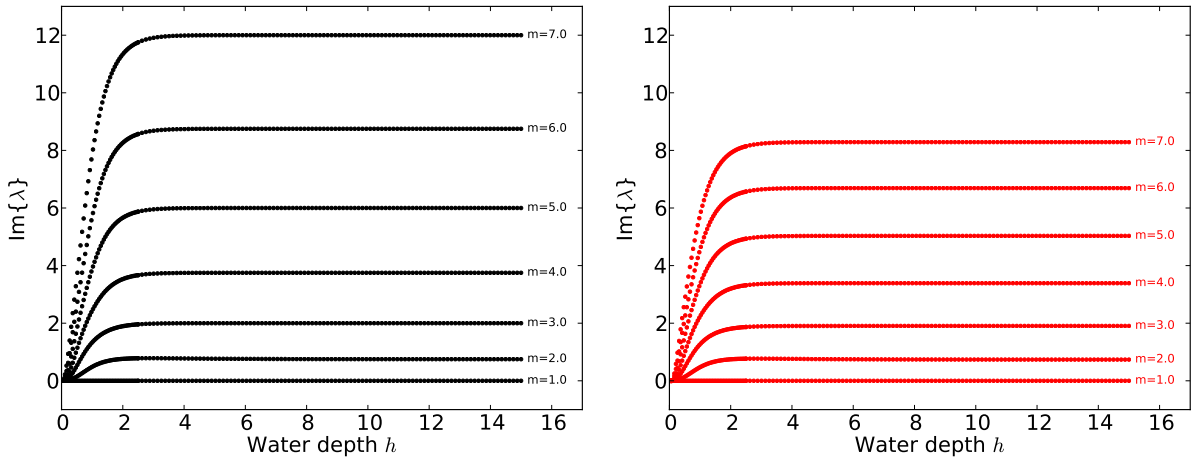

(a) (b)

Figure 6: The imaginary part of the eigenvalues for which the collision condition is met as a function of depth h. On the left the case of gravity waves ($\sigma = 0$) is displayed. The case $\sigma = 1/(90\pi)$ is shown on the right. Different curves correspond to different values of m. Negative values would result in the mirror imagine of this figure below the horizontal axis.

	$h = 0.5$				$h = 1.5$				$h = \infty$			
	$\sigma = 0$		$\sigma = 1/90\pi$		$\sigma = 0$		$\sigma = 1/90\pi$		$\sigma = 0$		$\sigma = 1/90\pi$	
m	μ	Im$\{\lambda\}$	μ	Im$\{\lambda\}$	μ	Im$\{\lambda\}$	μ	Im$\{\lambda\}$	μ	Im$\{\lambda\}$	μ	Im$\{\lambda\}$
1	0	0	0	0	0	0	0	0	0	0	0	0
2	0.106	0.148	0.100	0.139	0.322	0.687	0.314	0.673	0.25	0.75	0.243	0.736
3	0.375	0.519	0.345	0.478	-0.108	1.730	-0.157	1.651	0	2	-0.065	1.904
4	-0.206	1.088	-0.292	0.973	-0.095	3.188	-0.316	2.900	0.25	3.75	-0.028	3.389

Table 1: This table gives the Floquet parameters μ for which we have an eigenvalue collision in the case of flat water. The approximate values shown here are for the test cases we consider in the numerical results section, presenting only those Floquet parameters for which the largest instabilities are expected.

and imaginary axis. This is only possible through eigenvalue collisions, which are a necessary condition for the development of instabilities [29]. Thus we examine for which parameter values different eigenvalues given by (30) collide. This was originally investigated by MacKay and Saffman [30], who found that eigenvalues with the same sign s do not collide. Otherwise the collision condition becomes

$$\lambda_{\mu}^{s_1} = \lambda_{\mu+m}^{s_2} \quad \text{for any } m \in \mathbb{Z}, s_1 \neq s_2. \tag{31}$$

This equation determines for which Floquet exponents μ (modulo 1) eigenvalues collide, depending on different parameters h, g, σ. Figure 5 displays values of μ for which (31) is satisfied, as a function of the depth h, for fixed g and σ ($\sigma = 0$ in black, and $\sigma = 1/(90\pi)$, in red). The different curves correspond to different values of m.

Figure 6 shows the positive imaginary part of the collision points (their real part is zero) as a function of the water depth for $\sigma = 0$ (left) and $\sigma = 1/(90\pi)$ (right). Table 1 compares such imaginary parts computed for different depths h with and without surface tension. One of the goals for examining the

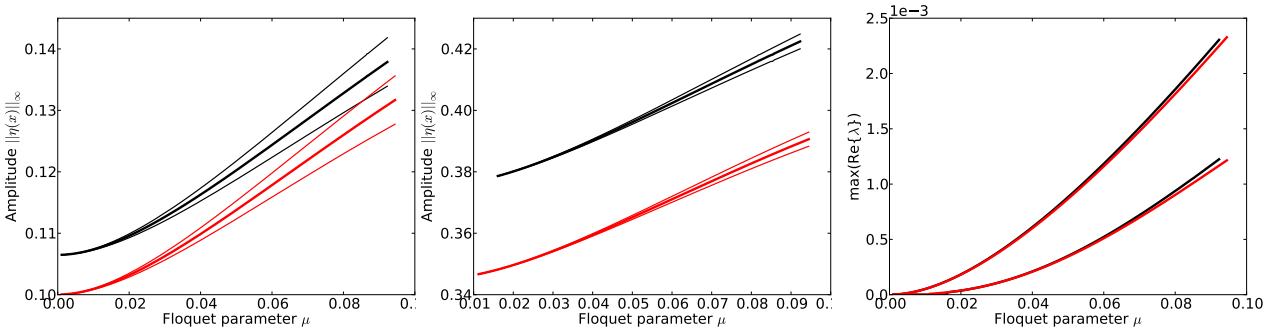

(a) (b) (c)

Figure 7: Tracking the bubble location and width as a function of solution amplitude, with curves in black for $\sigma = 0$, curves in red for $\sigma = 1/(90\pi)$. The left panel tracks the largest bubble, the middle panel the second largest. Their instability growth rates are shown on the right.

spectral stability of non-zero amplitude traveling wave profiles is to track whether the collided eigenvalues do result in instabilities, and if so, how these evolve for solutions of higher amplitude.

5.3 Numerical Procedure

We proceed to solve the generalized eigenvalue problem (28) using the Floquet-Fourier-Hill method [14, 15] for a sufficient number of values of the Floquet exponent μ to ensure all features of the spectrum are resolved. This is done in part by tracking (see below) the location of instabilities of solutions of smaller amplitude, as we continue up the solution branch. The collided eigenvalues of the flat water state are the starting point for this. As discussed below, we find that *all* traveling water waves are spectrally unstable, irrespective of their amplitude and of the depth of the water. This result is not surprising for waves in deep water, where the presence of the Benjamin-Feir instability [6] is well known. Deconinck and Oliveras [15] computed bubbles of instability (*i.e.*, topological ovals of spectral elements across the imaginary axis, which emanate from the flat-water collided eigenvalues for small wave amplitude), but these bubbles are narrow and it was reasonable to hope that the inclusion of surface tension might prevent their formation, leading to spectrally stable wave profiles for at least some amplitude and depth range. This is not the case. The goal of this and the following subsections is to demonstrate how surface tension affects the results of [15], while it cannot overcome the instabilities. For the three values of depth h in Figure 3, we examine the Floquet parameter μ for which instabilities are present, as well as the graph of the spectrum in the complex λ plane. We can do so along the entire solution branch in Figure 3. The figures included results only for the solution labeled with a square in Figure 3, roughly in the middle of the computed branch.

5.4 Bubble Tracking

It is interesting to note that the center of the bubbles of instability are not given by the collision values of Table 1. The locations of the bubbles move as we increase the amplitude of the traveling waves. We can track the movement of the center of the bubbles as well as of their width numerically, as shown in Figure 7. This was done for shallow water bubbles, since the bubbles are most important there. In Figure 7a-b, we track the movement of the largest and second-largest bubble of instability, respectively. As usual, black curves correspond to $\sigma = 0$, red ones to $\sigma = 1/(90\pi)$. Lastly, Figure 7c shows the change in the size of the bubble *i.e.*, its associated instability growth rate) as a function of the solution amplitude, hence the largest bubble corresponds to the top curves, the second bubble to the bottom curves. The rapid movement of the bubbles presents a numerical difficulty that needs to be overcome with a careful choice of the Floquet

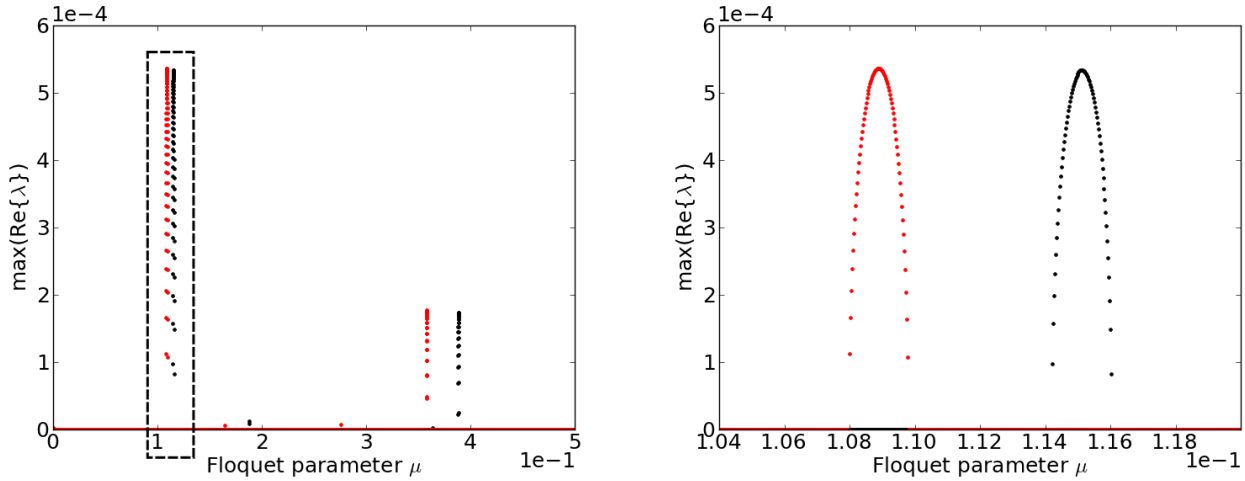

Figure 8: The maximal growth rate $\max \mathrm{Re}(\lambda)$ as a function of the Floquet exponent μ for $h = 0.5$ (shallow water). Throughout, black dots correspond to $\sigma = 0$, while red dots are for $\sigma = 1/(90\pi)$. Nonzero $\max \mathrm{Re}(\lambda)$ denote instabilities. The right panel is a zoom of the indicated region of the left panel.

exponents used in order to resolve all relevant features of the stability spectrum.

5.5 Stability Spectra

Figures 8-10 display the maximal real part of the spectral elements as a function of the Floquet parameter μ. Nonzero values correspond to instabilities. The results for shallow water ($h = 0.5$) are in Figure 8. They illustrate that the effect of surface tension is to shift for which Floquet exponents instabilities occur, while barely affecting their growth rate. The zoom on the right shows that the numerical results are well resolved and that the sharp spikes on the left lie above a range of μ values for which instabilities are present. As the wave amplitude is decreased, the width of these ranges shrinks to zero, approaching one of the values of μ for which eigenvalues collide for the flat water state. Different instabilities are visible, with a wide variety of instability growth rates. Figure 9 shows the result for deep water ($h = 1.5$) and Figure 10 shows the result for infinitely deep water ($h = \infty$), where the results are dominated by the Benjamin-Feir instability, as in [15]. Although the Benjamin-Feir instability is affected by the inclusion of surface tension, it appears to be affected much less than the bubbles, which are still present, but whose location may be shifted significantly.

In shallow water without surface tension, Deconinck and Oliveras [15] found the bubbles of instability shown in the first row of Figure 11. Two zooms of the complex λ plane shown on the left are shown there, demonstrating the absence of any instability at the origin (middle) and an enlargement of the bubble corresponding to the dominant instability (right). If surface tension is included, the results change as shown in the second row of Figure 11. The location of the bubbles changes, as remarked above. The largest real part is slightly increased, although this is hard to discern in Figure 11. The change in bubble location is a consequence of the change in eigenvalue collision location, displayed in Table 1. Importantly, more bubbles are visible with surface tension than without. This is illustrated in the second panel where two bubbles are shown to exist close to (but not at) the origin of the λ plane.

For waves in deep water ($h > 1.363$) [5, 39] without surface tension, both the bubble instabilities as well as the Benjamin-Feir instability appear. In terms of the largest growth rate of the instabilities, the Benjamin-Feir instability dominates for $h > 1.4306$, see [15]. A representative result is shown in the top row of Figure 12. The results with surface tension included are shown in the bottom row. Once again,

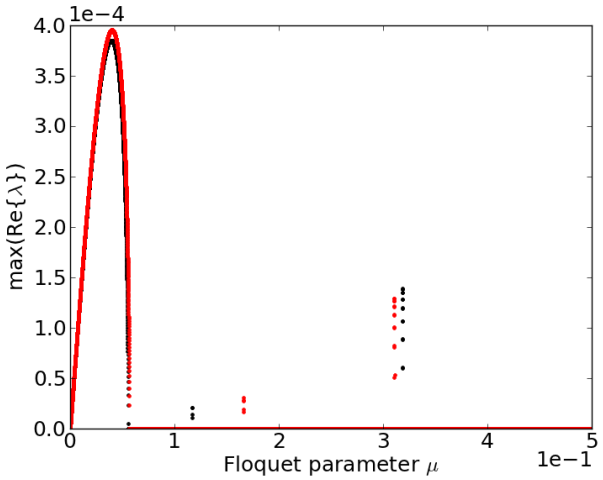

Figure 9: The maximal growth rate $\max \mathrm{Re}(\lambda)$ as a function of the Floquet exponent μ for $h = 1.5$ (deep water). Throughout, black dots correspond to $\sigma = 0$, while red dots are for $\sigma = 1/(90\pi)$. Nonzero $\max \mathrm{Re}(\lambda)$ denote instabilities.

the growth rates are slightly higher with surface tension than without. This is more obvious in Figure 8. Zooming into the center of the complex plane clearly shows the figure eight characteristic of the Benjamin-Feir instability, both with and without surface tension. However, with surface tension, two other facets are apparent. Zooming in one more time to resolve the pattern seen at the center, we see a bubble of instability quite clearly for $\sigma = 1/(90\pi)$, absent for pure gravity waves. Another feature is the splitting of the Benjamin-Feir figure eight, away from the origin. This occurs for gravity waves as well, but it appears to happen for gravity-capillary waves for traveling waves of significantly lower amplitude.

Finally, the case of infinite depth is examined in Figure 13. As before, the results for pure gravity waves ($\sigma = 0$) are shown in the top row, those with $\sigma = 1/(90\pi)$ in the bottom row. Once again, the Benjamin-Feir instability and bubble instabilities are observed. The Benjamin-Feir instability is even more dominant than before, as shown in Figure 13. Both with and without surface tension, the bubbles can barely be seen. As for $h = 1.5$, zooming into the origin, shows that the Benjamin-Feir instability has split away from the origin for a traveling wave of this amplitude.

6 Conclusions

We have investigated the effect of small surface tension on the spectral stability of the one-dimensional evolution of periodic traveling water waves within the context of the classical Euler equations governing potential flow. First, we used numerical continuation to extend the results of [15] by computing traveling wave solutions of the Euler equations in the presence of surface tension. This was done using the water wave formulation of Ablowitz, Fokas, and Musslimani [1], and care was taken to avoid resonant or near-resonant waves.

With these solutions in hand, we numerically computed their stability spectrum using the Floquet-Fourier-Hill method [14], ensuring that all relevant aspects of the spectrum were captured. To this end, we tracked the location of the bubbles of instability that originate from collided eigenvalues in the flat water state. We found that the inclusion of surface tension does not overcome the formation of the bubbles, so that all periodic traveling waves of the water wave problem are spectrally unstable. For pure gravity waves ($\sigma = 0$), this conclusion was already reached in [15], which focuses on the one-dimensional problem, and it

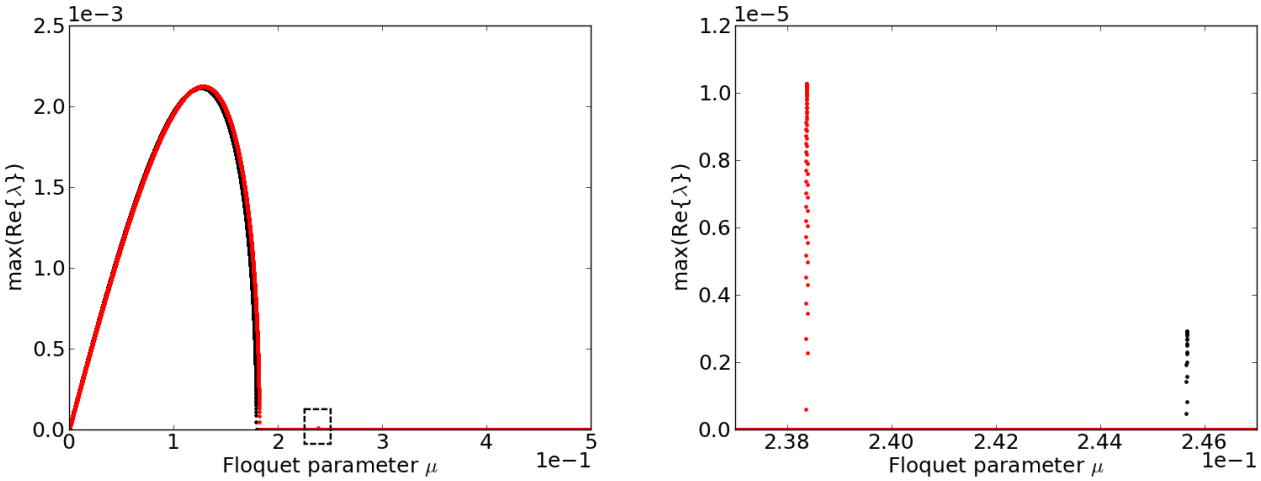

(a) (b)

Figure 10: The maximal growth rate $\max \mathrm{Re}(\lambda)$ as a function of the Floquet exponent μ for $h = \infty$ (infinitely deep water). Throughout, black dots correspond to $\sigma = 0$, while red dots are for $\sigma = 1/(90\pi)$. The right panel is a zoom of the indicated region of the left panel.

can be inferred from restricting the two-dimensional studies of [31, 17] to one spatial dimension by allowing only one-dimensional perturbations. In fact, with surface tension, the growth rates observed are somewhat larger than those seen without. Our instability conclusion holds for both shallow and deep water. In shallow water, the bubbles appear to be the only mechanism for instability, while in deep water the Benjamin-Feir or modulational instability is typically dominant.

Acknowledgements

This work was generously supported by the National Science Foundation under grant NSF-DMS-1008001. Olga Trichtchenko also acknowledges support from the Natural Sciences and Engineering Research Council of Canada, through a graduate fellowship. Any opinions, findings, and conclusions or recommendations expressed in this material are those of the authors and do not necessarily reflect the views of the funding sources.

This work has benefitted from conversations with Benjamin Akers and with Katie Oliveras. Both are thanked for their feedback and input.

References

[1] M. J. Ablowitz, A.S. Fokas, and Z.H. Musslimani. On a new non-local formation of water waves. *J. Fluid Mech.*, 562:313–343, 2006.

[2] B. Akers and D. P. Nicholls. Traveling waves in deep water with gravity and surface tension. *SIAM J. Appl. Math.*, 70:2373–2389, 2010.

[3] B. Akers and D. P. Nicholls. Spectral stability of deep two-dimensional gravity water waves: repeated eigenvalues. *Submitted for publication*, pages 1–19, 2012.

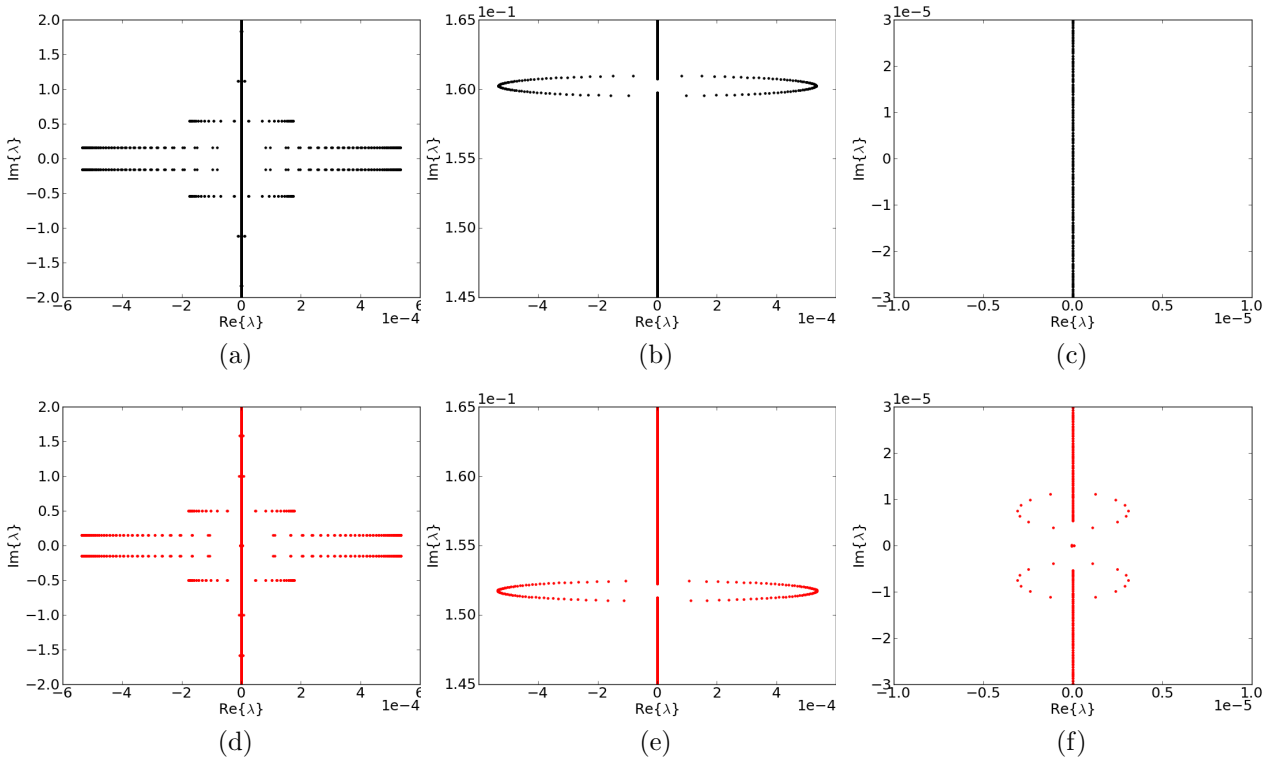

Figure 11: The complex λ plane for waves in shallow water (h=0.5), without (top) and with (bottom) surface tension. A discussion is presented in the main text.

[4] G. K. Batchelor. *An introduction to fluid dynamics*. Cambridge Mathematical Library. Cambridge University Press, Cambridge, paperback edition, 1999.

[5] T. B. Benjamin. Instability of periodic wavetrains in nonlinear dispersive systems. *Proc. Roy. Soc. (London) Ser. A*, 299:59–76, 1967.

[6] T. Brooke Benjamin and J. E. Feir. The disintegration of wave trains on deep water. *J. Fluid Mech.*, 27:417–430, 1967.

[7] Harald Bohr. *Almost Periodic Functions*. Chelsea Publishing Company, New York, N.Y., 1947.

[8] D. C. Calvo, T.-S. Yang, and T. R. Akylas. On the stability of solitary waves with decaying oscillatory tails. *R. Soc. Lond. Proc. Ser. A Math. Phys. Eng. Sci.*, 456(1995):469–487, 2000.

[9] A. Constantin and W. Strauss. Pressure beneath a Stokes wave. *Comm. Pure Appl. Math.*, 63:533–557, 2010.

[10] W. Craig and C. Sulem. Numerical simulation of gravity waves. *J. Comput. Phys.*, 108:73–83, 1993.

[11] A. D. D. Craik. The origins of water wave theory. *Annu. Rev. Fluid Mech.*, 36:1–28, 2004.

[12] G. D. Crapper. An exact solution for progressive capillary waves of arbitrary amplitude. *J. Fluid Mech.*, 2:532–540, 1957.

[13] C. W. Curtis and B. Deconinck. On the convergence of hill's method. *Maths. of Computations*, 79:169–187, 2010.

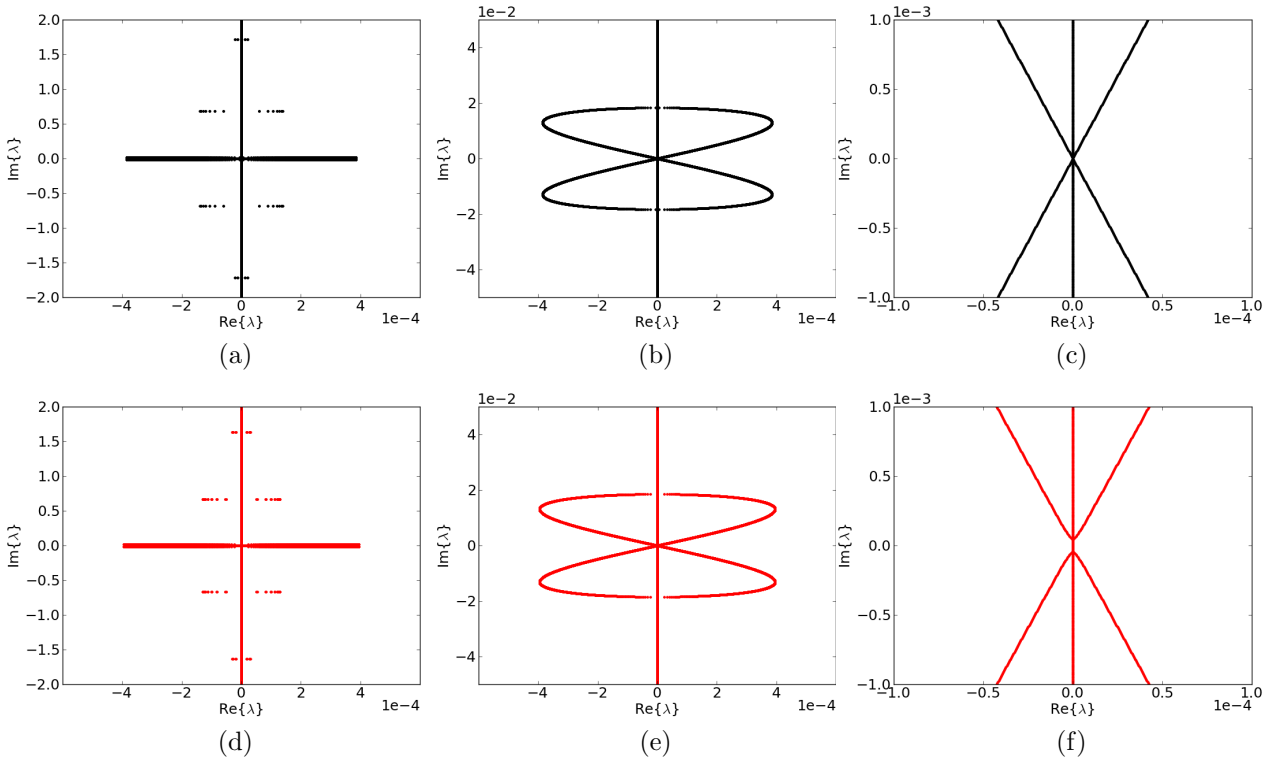

Figure 12: The complex λ plane for waves in deep water (h=1.5), without (top) and with (bottom) surface tension. A discussion is presented in the main text.

[14] B. Deconinck and J. N. Kutz. Computing spectra of linear operators using the Floquet-Fourier-Hill method. *Journal of Comp. Physics*, 219:296–321, 2006.

[15] B. Deconinck and K. Oliveras. The instability of periodic surface gravity waves. *J. Fluid Mech.*, 675:141–167, 2011.

[16] E.J. Doedel, R.C. Paffenroth, A.R. Champneys, T.F. Fairgrieve, Yu.A. Kuznetsov, B. Sandstede, and X. Wang. AUTO 2000: Continuation and bifurcation software for ordinary differential equations (with HomCont), 2001. http://indy.cs.concordia.ca/auto/.

[17] M. Francius and C. Kharif. Three-dimensional instabilities of periodic gravity waves in shallow water. *J. Fluid Mech.*, 561:417–437, 2006.

[18] W. Govaerts and Y. A. Kuznetsov. MatCont, 2007. http://matcont.sourceforge.net/.

[19] J. L. Hammack and D. M. Henderson. Resonant interactions among surface water waves. *Annual review of fluid mechanics*, 25:55–97, 1993.

[20] P. D. Hislop and I. M. Sigal. *Introduction to spectral theory*, volume 113 of *Applied Mathematical Sciences*. Springer-Verlag, New York, 1996. With applications to Schrödinger operators.

[21] E. L. Ince. *Ordinary Differential Equations*. Dover Publications, New York, 1944.

[22] M. A. Johnson and K. Zumbrun. Convergence of Hill's method for nonselfadjoint operators. *SIAM J. Numer. Anal.*, 50(1):64–78, 2012.

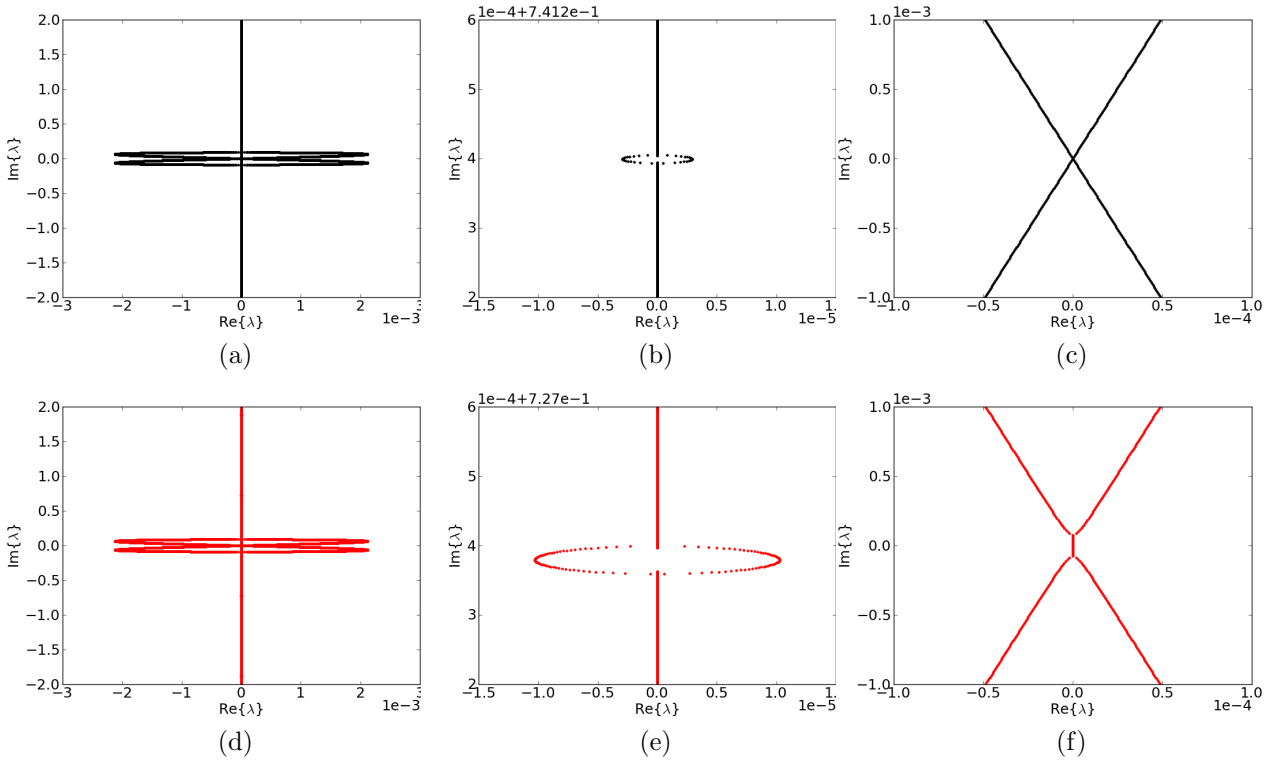

Figure 13: The complex eigenvalue plane showing bubble instabilities in water of infinite depth, $\sigma = 1/90\pi$ in red and $\sigma = 0$ in black.

[23] B. Kim and T. R. Akylas. Transverse instability of gravity-capillary solitary waves. *J. Engrg. Math.*, 58(1-4):167–175, 2007.

[24] T. Levi-Civita. Détermination rigoreuse des ondes permanentes d'ampleur finie. *Math. Ann.*, 93:264, 1925.

[25] M. S. Longuet-Higgins. The instabilities of gravity waves of finite amplitude in deep water. I. Superharmonics. *Proc. Roy. Soc. London Ser. A*, 360:471–488, 1978.

[26] M. S. Longuet-Higgins. The instabilities of gravity waves of finite amplitude in deep water. II. Subharmonics. *Proc. Roy. Soc. London Ser. A*, 360:489–505, 1978.

[27] M. S. Longuet-Higgins. Capillary-gravity waves of solitary type and envelope solitons on deep water. *J. Fluid Mech.*, 252:703–711, 1993.

[28] M. S. Longuet-Higgins and E. D. Cokelet. The deformation of steep surface waves on water. I. A numerical method of computation. *Proc. Roy. Soc. London Ser. A*, 350:1–26, 1976.

[29] R. S. MacKay. Stability of equilibria of Hamiltonian systems. In *Nonlinear phenomena and chaos (Malvern, 1985)*, Malvern Phys. Ser., pages 254–270. Hilger, Bristol, 1986.

[30] R. S. MacKay and P.G. Saffman. Stability of water waves. *Proc. R. Soc. London A*, 406:115–125, 1986.

[31] J. W. McLean. Instabilities of finite-amplitude water waves. *J. Fluid Mech.*, 114:315–330, 1982.

[32] P. A. Milewski, J.-M. Vanden-Broeck, and Z. Wang. Dynamics of steep two-dimensional gravity–capillary solitary waves. *J. Fluid Mech.*, 664:466–477, 2010.

[33] A. I. Nekrasov. *Točnaya teoriya voln ustanovivšegocya vida na poverhnosti tyaželoĭ židkosti.* Izdat. Akad. Nauk SSSR, Moscow, 1951.

[34] E. I. Părău, J.-M. Vanden-Broeck, and M. J. Cooker. Nonlinear three-dimensional gravity-capillary solitary waves. *J. Fluid Mech.*, 536:99–105, 2005.

[35] G. B. Stokes. On the theory of oscillatory waves. *Mathematical and Physical Papers*, 1:197–229, 1847.

[36] D. J. Struik. Détermination rigoreuse des ondes irrotationnelles priodiques dans un canal profondeur finie. *Math. Ann.*, 95:595, 1926.

[37] R. Tiron and W. Choi. Linear stability of finite-amplitude capillary waves on water of infinite depth. *J. Fluid Mech.*, 696:402–422, 2012.

[38] J.-M. Vanden-Broeck. *Gravity-Capillary Free-Surface Flows.* Cambridge University Press, Cambridge, 2010.

[39] G. B. Whitham. Non-linear dispersion of water waves. *J. Fluid Mech.*, 27:399–412, 1967.

[40] J.R. Wilton. On ripples. *Philosophical Magazine Series 6*, 29(173):688–700, 1915.

[41] V. E. Zakharov. Stability of periodic waves of finite amplitude on the surface of a deep fluid. *J. Appl. Mech. Tech. Phys.*, 9:190–194, 1968.

[42] J. Zhang and W. K. Melville. On the stability of weakly-nonlinear gravity-capillary waves. *Wave Motion*, 8(5):439–454, 1986.